1-15-2015

Peat Formation Concentrates Arsenic Within Sediment Deposits of the Mekong Delta

Jason W. Stuckey
Stanford University

Michael V. Schaefer
Stanford University

Benjamin D. Kocar
Massachusetts Institute of Technology

Jessica Dittmar
Stanford University

Juan Lezama Pacheco
Stanford University

See next page for additional authors

Publication Information

Stuckey, Jason W.; Schaefer, Michael V.; Kocar, Benjamin D.; Dittmar, Jessica; Pacheco, Juan Lezama; Benner, Shawn G.; and Fendorf, Scott. (2015). "Peat Formation Concentrates Arsenic within Sediment Deposits of the Mekong Delta". *Geochimica et Cosmochimica Acta, 149*, 190-205.http://dx.doi.org/10.1016/j.gca.2014.10.021

Authors
Jason W. Stuckey, Michael V. Schaefer, Benjamin D. Kocar, Jessica Dittmar, Juan Lezama Pacheco, Shawn G. Benner, and Scott Fendorf

Peat Formation Concentrates Arsenic within Sediment Deposits of the Mekong Delta

Jason W. Stuckey[a], Michael V. Schaefer[a], Benjamin D. Kocar[b], Jessica Dittmar[a], Juan Lezama Pacheco[a], Shawn G. Benner[c], and Scott Fendorf[a,*]

[a]*Department of Environmental & Earth System Science*
Stanford University, Stanford, CA 94305

[b]*Parsons Laboratory*
Massachusetts Institute of Technology, Cambridge, MA 02139

[c]*Department of Geosciences*
Boise State University, Boise, ID 83725

**Corresponding author. Tel.: +650 723 5238*
E-mail address: fendorf@stanford.edu

Abstract

Mekong River Delta sediment bears arsenic that is released to groundwater under anaerobic conditions over the past several thousand years. The oxidation state, speciation, and distribution of arsenic and the associated iron bearing phases are crucial determinants of As reactivity in sediments. Peat from buried mangrove swamps in particular may be an important host, source, or sink of arsenic in the Mekong Delta. The total concentration, speciation, and reactivity of arsenic and iron were examined in sediments in a Mekong Delta wetland by X-ray fluorescence spectrometry (XRF), X-ray absorption spectroscopy (XAS), and selective chemical extractions. Total solid-phase arsenic concentrations in a peat layer at a depth of 6 m below ground increased 10-fold relative to the overlying sediment. Extended X-ray absorption fine structure (EXAFS) spectroscopy revealed that arsenic in the peat was predominantly in the form of arsenian pyrite. Arsenic speciation in the peat was examined further at the micron-scale using μXRF and μX-ray absorption near-edge structure (XANES) spectroscopy coupled with principal component analysis. The multiple energy μXRF mapping and μXANES routine was repeated for both iron and sulfur phase analyses. Our μXRF/μXANES analyses confirm arsenic association with pyrite – a less reactive host phase than iron (hydr)oxides under anaerobic conditions. The arsenian pyrite likely formed upon deposition/formation of the peat in a past estuarine environment (~ 5.5 ka BP), a process that is not expected under current geochemical conditions. Presently, arsenian pyrite is neither a source nor a sink for aqueous arsenic in our sediment profile, and under present geochemical conditions represents a stable host of As under the reducing aquifer conditions of the Mekong Delta.

Furthermore, organic carbon within the peat is unable to fuel Fe(III) reduction, as noted by the persistence of goethite which can be reduced microbially with the addition of glucose.

1. INTRODUCTION

Human exposure to arsenic through domestic use of groundwater in South and Southeast Asia starts with the weathering of Himalayan As-bearing rock in basin headwaters, followed by riverine transport and deposition into Holocene aquifers (Saunders et al., 2005). Arsenic concentrations in basin groundwater commonly exceed the 10 μg As L^{-1} World Health Organization standard by more than 10-fold (Smedley and Kinniburgh, 2002). Consumption of arsenic-contaminated groundwater has led to the chronic poisoning of tens of millions of people in the Bengal Basin of West Bengal and Bangladesh (Ahmed et al., 2006; Chatterjee et al., 1995; Ravenscroft et al., 2009; Sambu and Wilson, 2008; Yu et al., 2003). The widespread use of tube wells for drinking water supply has put millions more at risk in the Red River (northern Vietnam) and Mekong Deltas (Cambodia and southern Vietnam) (Berg et al., 2007).

The biogeochemical cycling of iron, sulfur, and carbon (in natural organic matter) largely control the partitioning and speciation of arsenic in these deltaic sediments. Under anaerobic conditions, microbially driven oxidation of organic matter coupled to the dissimilatory reductive dissolution of As-bearing iron (hydr)oxides causes the transfer of arsenic from the solid to the aqueous phase (Akai et al., 2004; Islam et al., 2004; McArthur et al., 2001; Nickson et al., 1998; Nickson et al., 2000; Van Geen et al., 2004).

Reductive dissolution of As(V)-bearing Fe(III) (hydr)oxides is the dominant mechanism by which aqueous concentrations of arsenic, and its resulting transport, are increased (Dixit and Hering, 2003; Fendorf and Kocar, 2009; Kocar et al., 2008; Postma et al., 2007; Smedley and Kinniburgh, 2002; Tufano et al., 2008).

In addition to Fe(III), sulfate is an important electron acceptor linked to organic carbon oxidation in anaerobic microbial respiration, and sulfide precipitation may act as solid-phase sink for arsenic. In combination with pH, the mineralogical form of Fe(III) (hydr)oxides determines the relative favorability of iron and sulfate reduction, and the two terminal electron accepting processes often occur simultaneously (Buschmann and Berg, 2009; Kocar and Fendorf, 2009; Postma and Jakobsen, 1996). Stoichiometric iron and sulfate reduction can lead to the formation of $FeS_{(s)}$ (e.g., mackinawite) and subsequent adsorption of As or the co-precipitation of As-bearing iron sulfides (Buschmann and Berg, 2009; Couture et al., 2010; Couture et al., 2013a; Postma and Jakobsen, 1996). Iron monosulfides are often precursors to pyrite ($FeS_{2(s)}$) in low-temperature geochemical environments (Morse and Rickard, 2004; Rickard, 1997; Rickard and Luther, 1997; Rickard, 1975), and may lead to arsenian pyrite ($Fe(S,As)_2$) (Lowers et al., 2007; Savage et al., 2000), or arsenopyrite (FeAsS) (Bostick and Fendorf, 2003). Alternatively, pyrite may form by heterogeneous nucleation without FeS precursors on iron-rich clay minerals (Lowers et al., 2007). Indeed, As-bearing iron sulfides, including arsenian pyrite, are present in Bengal Basin (Bangladesh) sediments (Lowers et al., 2007; Polizzotto et al., 2005). Adequate sediment sulfur (sulfate) supply and reaction time allow for authigenic arsenian pyrite formation with arsenic incorporation up to 1.3 % (Lowers et al., 2007). The extent to which pyrite incorporates structural arsenic increases with decreased pyrite growth rate, higher As:S ratios in solution, and/or a higher

dissolved As concentration (Bostick and Fendorf, 2003; Fleet et al., 1989; Lowers et al., 2007). Non-Fe-bearing arsenic sulfides may scavenge As from solution as well. When arsenic reaches micro-molar levels under sulfate-reducing conditions, realgar (AsS) is the first As sulfide to precipitate in circumneutral pH environments with high Fe^{2+}, low HS^-/H_2S activities, whereas orpiment (As_2S_3) stability is predicted at low Fe^{2+}, high HS^-/H_2S conditions (O'Day et al., 2004). Thus, arsenic partitioning with sulfide minerals is a function of several environmental factors in sediment/soil systems including redox state, temperature, and activities of H^+, Fe^{2+}, and HS^-/H_2S.

Buried natural organic matter or peat is implicated as the fuel for reductive dissolution of arsenic-bearing iron (hydr)oxides, leading to As release in the Bengal Basin (McArthur et al., 2004; McArthur et al., 2010; McArthur et al., 2011; McArthur et al., 2008; McArthur et al., 2001). Peat may potentially drive arsenic release locally and/or produce dissolved organic carbon (DOC), which may stimulate As release down gradient in the aquifer (McArthur et al., 2008). However, peat often has sulfur-containing functional groups, particularly of marine or estuarine origin, with a strong affinity for arsenic (Langner et al., 2012). Peat also facilitates the formation of potentially stable arsenian pyrite in anoxic sediments through microbially mediated processes (Huertadiaz and Morse, 1992; Schoonen, 2004). Thus, the role of peat in regulating arsenic partitioning, reactivity, and mobility in sediments of the As-impacted deltas of S/SE Asia is complex and unresolved. Here we seek to *(1)* define the speciation of arsenic, iron, and sulfur in the peat found in near-surface sediments (upper 10 m) of the Mekong Delta, *(2)*, determine the reactivity of the peat-associated arsenic, and *(3)* determine whether buried peat is a source or sink for arsenic relative to groundwater in deltaic sediments. We complement

field measurement with laboratory incubation studies to define the processes controlling arsenic partitioning within the near-surface sediments.

2. MATERIALS AND METHODS

2.1. Field area

The Mekong River currently traces a 4600 km course from its headwaters in the Himalaya (Tibet) to the South China Sea (Hori, 2000). The modern Mekong Delta initiated at 8.4 ka following a period of rapid sea-level rise and aggradation of the fluvial system (Tamura et al., 2009). Sea-level rise decelerated for the subsequent ~ 2000 years, producing aggrading to prograding tidal flats and mangrove forests and resultant peat layers in the sediment profile of the present-day upper Mekong Delta (Tamura et al., 2009). Rapid progradation of the delta has occurred from 6.3 ka to the present, with the highest sediment accumulation rates ensuing in the past 0.6 to 1 ka (Tamura et al., 2009).

Our field area spans 50 km^2 of the upper Mekong Delta in Kandal Province, Cambodia, and is bracketed by the Mekong and Bassac rivers (Lat. 11 31 3.90N, Long. 105 0 41.77E) (Polizzotto et al., 2008). Elevated levees along the riverbanks give way to native wetlands between the two rivers. The general stratigraphy of the field area is approximately 15 m of clays overlying > 30 m of aquifer-forming sands (Benner et al., 2008). The annual monsoon causes the river stage to breach the levees, resulting in deposition of floodwater and arsenic-bearing sediments into the wetland basin. The hydraulic head of the interior surface wetlands exceeds that of

the Mekong River throughout the year except for the latter part of the rainy season (roughly July through October) (Benner et al., 2008; Polizzotto et al., 2008). The fine-over-coarse stratigraphy and fluctuating hydraulic gradient result in a net annual flow velocity of 0.04 – 0.4 ma^{-1} vertically through the clay and 1 – 13 ma^{-1} horizontally through the aquifer sands toward the Mekong River (Benner et al., 2008).

The monsoon-driven flooding of the wetland basin between the Mekong and Bassac rivers is generally seasonal, except in topographically low abandoned river channel (oxbow) wetlands. Permanent flooding in the oxbow wetlands leads to arsenic release (solid to solution transfer) in the surface clay aquitard and subsequent downward transport to the sandy aquifer where groundwater concentrations reach up to 16 µM As (Polizzotto et al., 2008). In a previously studied oxbow wetland within our field area, lysimeter-collected mean pore-water arsenic concentrations are 0.7 – 0.9 µM at 1 and 2 m depth, and well water As concentrations are more than 2.5 – 8 µM at 7 m (Kocar et al., 2008). The site of the current study is seasonally flooded, and has lysimeter-collected pore-water arsenic concentrations of < 0.1 µM at depths of 1.1 and 1.5 m and well water As concentrations are 0.2 µM at 7.5 m. Hence, aqueous arsenic concentrations increase with depth within the near-surface clays in both depositional environments, though to a lesser degree in the seasonally flooded wetland.

The stratigraphy of the clay aquitard of the site for the current study is comprised of alternating reddish brown (Munsell color 5YR 6/3) (natural levee) and gray (2.5Y 4/1 – 2.5Y 6/1) (floodplain) strata down to a depth of 6 m with an organic-rich (5.4 % C) dark

gray (2.5Y 3/1) layer between 5.4 and 5.6 m (Fig. A.1). A black (2.5Y 2.5/1) peat layer (21.5 % C) is present between 6.0 and 6.1 m (Table 1; Fig. A.1). The mean solid-phase arsenic concentration averaged across the top 6 m is 15.8 ± 4.7 mg As kg^{-1}.

2.2. Sediment collection and analysis.

An excavator was used to dig to a depth of 6.5 m. Aluminum cores were pounded into a fresh sediment face, immediately sealed with wax, vacuum sealed in a bag containing an anaerobic pouch (Mitsubishi Gas Chemical America, Inc.), placed on ice in the field and stored at 4 °C. Three sediment cores were retrieved per depth.

Total elemental composition was determined by X-ray fluorescence spectrometry (XRF), and sediment pH was measured in 0.01 M $CaCl_2$•H_2O (Dittmar et al., 2007). Total C and N analysis was performed on two different samples for each depth using a Carlo-Erba NA 1500 Elemental Analyzer. The groundwater is undersaturated with respect to calcite (Kocar et al., 2008). Saturation of Fe^{2+}(aq) with respect to siderite is thermodynamically favorable in our sediment profile; however, siderite ($FeCO_{3\ cryst}$) is not detected by XRD in the near surface (top 6.5 m) (e.g., Figs. A.2 and A.3). Thus, the total C values are representative of the organic C content in these acidic sediments, in which carbonate precipitation is minimal.

Sediment age was determined by ^{14}C dating. Sediment cores were collected in copper pipe, immediately shock frozen in liquid nitrogen in the field, and preserved for ^{14}C analysis at the Keck Carbon Cycle Accelerator Mass Spectrometer facility at University of California Irvine. Samples were combusted at 900 °C under vacuum for three hours in the presence of cupric oxide and silver wire,

and the resulting carbon dioxide was cryogenically purified and reduced to graphite for ^{14}C analysis. The calculation of $\Delta^{14}C$ was corrected for mass dependent isotopic fractionation by $\delta^{13}C$ determination.

2.3. Arsenic-doped goethite preparation.

Goethite was synthesized by oxidation of $FeCl_2 \bullet 4H_2O$ at pH 7 (Schwertmann and Cornell, 2000), identified by X-ray diffraction (XRD), and doped with As(V) to a final concentration of 169 mg As(V) $(kg\ FeOOH)^{-1}$ – corresponding to the molar arsenic-to-iron ratio found in South and Southeast Asian sediments (Kocar and Fendorf, 2009). The goethite suspension was N_2-purged (> 1 h/L) and autoclaved at 121°C and 18 psi for 1 h.

2.4. Batch incubation.

Incubations were initiated in the field immediately upon sample collection to determine whether As/Fe release from sediments was limited by the reactivity of organic carbon or As-bearing iron (hydr)oxides. Incubation of peat samples was conducted in glass serum vials containing N_2-purged (> 1 h/L) and sterile filtered (0.2 μm) groundwater medium buffered to pH 7.1 with a final composition of 2.7 mM KCl, 0.28 mM $MgSO_4$, 7.8 mM NaCl, 0.41 mM $CaCl_2 \bullet 2H_2O$, 0.018 mM NH_4Cl, and 10 mM PIPES. Prior to peat addition, three treatment additions to the groundwater medium were performed in triplicate: 10 mM glucose, As-loaded goethite, and 10 mM glucose + As-loaded goethite, along with an unamended control. The mass ratio of goethite to peat was 0.64:1. Each

treatment had an abiotic counterpart achieved by antibiotic addition (150 mg penicillin L^{-1}, 250 mg streptomycin L^{-1}, and 40 mg chloramphenicol L^{-1}). The incubation vials were purged with N_2 for at least 1 min after 5 cm^3 of peat was injected using a syringe. Samples of peat were weighed before and after oven drying at 105 °C for 48 h to determine the dry mass of peat added in each incubation.

The incubation vials were returned to the lab and continuously mixed on an end-over-end rotator at ~ 20 rpm. The batch incubations were sampled 4 times over a period of 40 d, with the initial sampling occurring ~ 24 h after sediment additions in order to achieve a homogeneous suspension. Entrance of oxygen into the incubation vials was limited during sampling by the following N_2-flushing techniques when a glovebag was unavailable. For each sampling point, an aliquot of the mixed suspension was extracted using an N_2-purged syringe and 16G needle, and dispensed into an N_2-purged, crimp-sealed 30 ml serum vial. The suspension was allowed to settle, and the supernatant was extracted and filtered through a 0.2 μm polyethersulfone syringe filter for aqueous chemical analysis. Alkalinity and pH were measured immediately as described for groundwater analysis (Electronic Annex). The remaining supernatant was acidified to ~ 2 % v/v with concentrated HNO_3 for elemental analysis by ICP-MS.

2.5. Total and HCl-extractable arsenic.

The sediment cores were extruded, dried under 95%N_2/5%H_2 atmosphere, and homogenized by mortar and pestle. A 1 M hydrochloric acid (HCl) extraction was performed in duplicate on two replicate sediments samples for each depth to quantify an

operationally defined "reactive" As pool, presuming this concentration of HCl invoked the dissolution of amorphous Fe/Mn oxides, acid volatile sulfides, and carbonates (Keon et al., 2001). A citrate-bicarbonate-dithionite (CBD) extraction was performed in duplicate on two replicate sediment samples of the peat, ostensibly dissolving all reducible iron present (Loeppert and Inskeep, 1996). The 1 M HCl and CBD extracts were measured by inductively coupled plasma optical emission spectrometry (Thermo ICAP 6300 Duo View Spectrometer). The instrument detection limit was 5 ppb. Standards used for ICP-MS calibration were within ± 5% of external standards. Quality control standards were analyzed at least once per 15 samples run to ensure a ≤ 5% deviation from the standard curve was maintained. Total arsenic concentrations were determined by XRF.

2.6. Bulk X-ray absorption spectroscopy.

Arsenic K-edge XAS was performed at beam line 11-2 at the Stanford Synchrotron Radiation Laboratory (SSRL). Energy selection was achieved with a Si (220) monochromator detuned 30 – 40 % for harmonic rejection, and energy calibration was performed by assigning a K-edge position of 11874.0 to a Na_3AsO_4 standard. Fluorescent X-rays were measured with a multi-element germanium detector. For As K-edge XANES spectroscopy, samples were packed into 2 mm thick polycarbonate slot mounts in Kapton tape (25 µm thickness). Least squares fitting of normalized XANES fluorescence spectra was optimized over a range of 11850 to 11890 eV using normalized spectra of six standards representing the potential As species within the sediments. Arsenic K-edge EXAFS spectroscopy was performed in a He-purged cyrostat at 25 K. Arsenic standards were sufficiently diluted in BN to achieve a

unit change in absorption across the K-edge. Arsenic standards were verified by powder XRD. Sample fluorescence and standard transmission spectra were averaged, background subtracted, and normalized using the program Athena (Ravel and Newville, 2005). A spline function was fit through the absorption envelope and subtracted from each spectrum. The resulting EXAFS function (χ) was transformed into *k*-space ($Å^{-1}$) and weighted by k^3. Least squares fitting of the χ function was performed over a *k* range of 1 to 15.5 $Å^{-1}$ in Athena.

Iron K-edge EXAFS spectroscopy was performed at beam line 11-2 at SSRL in fluorescence and transmission mode. Energy selection was maintained by a Si (220) monochromator detuned 40 – 50 % for harmonic rejection, and energy calibration was achieved by assigning a K-edge position of 7112.0 to a Fe foil. Fluorescent X-rays were measured with a Lytle detector fitted with a 3 μm thick Mn filter. The bulk peat sample was deposited on 0.2 μm cellulose nitrate filter paper and packed in Kapton tape (25 μm thickness). Least squares fitting of the Fe EXAFS (χ) function was performed over a *k* range of 3 to 13 $Å^{-1}$. The specific iron standards used for fitting were defined by a combination of electron microprobe/energy dispersive spectrometry and XRD.

Sulfur K-edge XANES spectroscopy was performed at beam line 4-3 at SSRL. Energy selection was maintained by a fully tuned Si (111) monochromator with harmonic rejection mirrors in place. Energy calibration was achieved by assigning the first white line of a $Na_2S_2O_3$ standard to 2472.02 eV. X-rays were measured with a Vortex detector in fluorescence mode. Samples and beam path were kept under He (g) purge to avoid loss of photon flux. Standard sulfur K-edge XANES spectra were collected, internally calibrated, and normalized to a dimethylsulfoxide spectrum as described previously (Almkvist et al., 2010). (See Figure A.4 for more

details on the normalization procedure.) Least squares fitting of normalized XANES fluorescence spectra was optimized over a range of 2465 to 2490 eV using the LINEST function in Microsoft Excel (Almkvist et al., 2010). The least squares fitting procedure first aimed to reproduce all the features of the spectra quantitatively using the smallest number of components and eliminating those contributing to less than 5 % of the sum, yielding fits with up to 4 components (Couture et al., 2013b). The fit with the lowest *R*-factor value was chosen as the final fit. The major types of sulfur compounds found in sediments/soils were included as standards in the fitting routine: pyrite (FeS_2), pyrrhotite (FeS), organic sulfides, elemental S, thiols, thiosulfate, sulfoxides, sulfites, sulfones, sulfonates, sulfate esters, and sulfates (Almkvist et al., 2010). The sulfur compounds contributing to the final fits for all S XANES performed included pyrite, organic sulfides, sulfoxides, and a sulfate ester (Figs. A.4 and A.5; Table A.1).

2.7. Micro X-ray fluorescence (μXRF) mapping and μXANES spectroscopy.

A section of peat from the intact core was dried under 95%N_2/5%H_2 atmosphere and fixed in EPOTEK 301_2FL epoxy. A thin section (30 μm thick) was prepared on a quartz slide under low O_2 and low temperature conditions (Spectrum Petrographics method X26A). Coarse-scale μXRF mapping and μXANES analysis were performed at beam line 10-2 at SSRL with a spot size of 25 μm in diameter. Finer-scale μXRF mapping and μXANES spectral acquisition were performed at beam line 2-3 at SSRL, equipped with KB focusing mirrors providing a spot size of 2 x 2 μm. Elemental maps were generated using a single-element Si drift Vortex detector; the sample was continuously rastered across the X-ray beam using a 5 μm pixel step-size and dwell time of 50 ms per pixel. Windowed counts of each element were isolated from the full X-ray fluorescence spectra and normalized to the intensity of the incident X-ray

beam (I_0). Energy was selected using a Si (111) double crystal monochromator and calibrated by assigning a K-edge position of 11874.0 to a Na_3AsO_4 standard. Based on μXANES spectra of six As standards representing the potential chemical species within the aquifer sediments, we mapped a region of the thin section at As K-edge energies of 11867, 11869, 11872, 11876, and 11881 eV. Using the SMAK routine (Webb, 2011), principal component analysis (PCA) was performed on dead time corrected maps to determine optimal locations for μXANES spectral analysis. Least squares fitting of normalized μXANES spectra was optimized from 11850 to 11890 eV in SIXPACK (Webb, 2005). Normalized μXANES fluorescence spectra of the As standards corresponding to the five As K-edge energies were used to fit the multiple energy μXRF maps in a non-negative linear least squares sense in SMAK (Mayhew et al., 2011).

We verified that the peat grains in the coarse As μXRF map (Fig. 4) were representative of the entire peat sample based on three main lines of evidence: *(1)* A coarse μXRF map of the entire peat thin section (Fig. A.6); *(2)* Coarser scale multi-energy μXRF mapping coupled to the As μXANES fitting routine revealed similar arsenic speciation to that observed in Fig. 5 (Fig. A.7); and *(3)* the two images in Fig. 4 each spanned roughly 50 % of the surface area of the entire peat grain.

The multiple energy μXRF mapping and μXANES spectral acquisition routine was repeated for iron phase analysis of the peat. Energy calibration was achieved by assigning a K-edge position of 7112.0 eV to a Fe foil standard. Based on μXANES spectra of standard iron-bearing sulfides, carbonates, silicates, and oxides, the five Fe K-edge mapping energies chosen were 7120, 7122, 7127, 7131, 7139 eV. Least squares fitting of μXANES spectra was optimized from 7110 to 7150 eV. The number of Fe standards used for

each fit was guided by PCA and variance analysis of the unknown μXANES spectra. The specific Fe standards used for fitting were defined by a combination of electron microprobe/energy dispersive spectroscopy and XRD, target transformation of standards based on the PCA, as well as by the "Cycle Fit" function in SIXPACK (Webb, 2005). The proportion of Fe(II) and Fe(III) bearing minerals in the resultant μXANES fit was used to estimate the Fe(II):Fe(III) ratio for a given point on the map. Normalized μXANES fluorescence spectra of pyrite – the representative Fe(II) standard – and goethite – the representative Fe(III) standard – corresponding to the five Fe K-edge energies were used to fit the multiple energy μXRF maps in a non-negative linear least squares sense to achieve a distribution map of Fe oxidation state (Mayhew et al., 2011).

Finally, using beam line 14-3 at SSRL, multiple energy μXRF mapping and μXANES spectral collection were performed for S analysis of the peat grains. Focusing mirrors provided a spot size of 5 x 5 μm and harmonic rejection. Energy was selected using a Si (111) double crystal monochromator, and calibrated by assigning the top of the white line of a Na_2SO_4 standard to 2483.0 eV. The sample was rastered identically as for arsenic and iron mapping: continuous mode, 5 μm step size, and 50 ms dwell time per pixel. The S K-edge mapping energies chosen based on preliminary μXANES spectra of various sulfur standards were 2460 (background), 2470, 2472, 2473.5, 2474.5, 2482.5, and 2500 (total fluorescence). Least squares fitting of normalized XANES fluorescence spectra was optimized over a range of 2465 to 2490 eV using normalized spectra of multiple standards representing the potential sulfur species within the sediments as described for bulk S XANES (Section 2.6).

Section 2.8. X-ray diffraction.

Synchrotron powder X-ray diffraction was performed at beam line 11-3 at SSRL with an incident beam energy of 12735 eV. Samples were prepared as described for bulk Fe EXAFS (Section 2.6). Peak identification was performed using JADE XRD Pattern Processing Ver. 6.5 (Materials Data, Inc., 2002).

3. RESULTS

3.1. Sediment profile characterization.

The top 3.0 m of sediment has a reddish brown (Munsell color of 5YR 6/3) hue. Gray (Munsell colors of 2.5Y 4/1 – 2.5Y 6/1) layers spanning 3.0 m to 4.0 m and 4.8 m to 5.4 m deep sandwich another brown (10YR 6/3) layer between 4.0 and 4.8 m deep. A dark gray (2.5Y 3/1) sediment layer spans 5.4 m to 5.6 m overlying a gray (2.5Y 6/1) layer extending to 6.0 m. Finally, a black (2.5Y 2.5/1) peat layer is present between 6.0 m and 6.1 m.

The total C content is elevated in the gray and black sediments relative to the layers with a brown hue. The total C % generally decreases with depth in the brown layers from 0.54 % at 0.26 m to ~ 0.28 % at 4.2 m – 4.6 m (Table 1). The total C concentration ranges from 0.49 % to 0.85 % in the gray layers and from 1.7 % to 21.5 % in the black layers (Table 1). The variability between replicate samples was ± 10 % or less for all but the total C measurement at 5.80 m (± 17 %), indicating the degree of heterogeneity in C concentration within each sediment layer.

The peat layer and overlying sediment profile developed within the last 5.7 ka (Table 2), indicating an average sediment accumulation rate of 1 m ka^{-1}, corroborating previous measurements of 1 – 3.3 m ka^{-1} for our field area over the past 6 ka (Polizzotto et al., 2008). Sediment age 0.5 m above the peat decreases to 3.8 ka (Table 2), indicating a relatively low sediment accumulation rate of 0.3 m ka^{-1} (see Electronic Annex) – within the range of 0.3 – 0.7 m ka^{-1} measured for a comparable floodplain facies unit near our field site (Tamura et al., 2009). As the profile transitions from gray floodplain sediments to the overlying brown natural levee sediments, the measured sediment accumulation rate generally increases to ≥ 1 m k a^{-1}.

3.2. Arsenic speciation and acid-extractability within near-surface sediments.

Arsenic is present as As(V) in the top ~ 4 m of the sediment profile in the seasonally flooded wetland, with As(III) appearing in roughly equal proportion to As(V) at 5 m depth (Fig. 1). Arsenic-bearing sulfides are present in the organic-rich (5.4 % C) dark gray sediment layer at 5.55 m and a black peat (21.5 % C) layer at 6.10 m. The average total As concentration of the sediment in the

top 6 m is 15.8 ± 4.7 mg As kg^{-1}, which increases 10-fold in the peat layer (6.0 – 6.1 m) to 153 mg As kg^{-1}. In addition, the percentage of the total arsenic that is acid-extractable (by 1 M HCl) averages 10.6 ± 2.6 % (1.60 ± 0.15 mg As kg^{-1}) in the top 6 m, and decreases to 0.9 % (1.38 ± 0.72 mg As kg^{-1}) in the peat layer.

3.3. Reactivity of peat toward As/Fe release

Arsenic release (solid to solution transfer) was not observed in incubations of peat with As-loaded goethite, 10 mM glucose, 10 mM glucose + As-loaded goethite, or unamended groundwater medium (pH 7.1) (Fig. 2). Goethite addition to the peat did not stimulate iron release, nor was aqueous Fe observed in the incubation of peat alone. However, aqueous iron was produced in both the glucose and glucose + goethite treatments.

3.4. Solid-phase arsenic speciation in peat

In addition to total and acid-extractable concentrations, we examine the oxidation state and chemical form of As in the peat. Least squares fitting of the bulk XANES shows a 94% contribution by As-bearing sulfides with arsenite (likely adsorbed) accounting

for the remaining 6% (Fig. 1). The white line energy position differentiates arsenite (AsO_3^{3-}), arsenate (AsO_4^{3-}), and arsenic-bearing sulfides. Owing to the small shift in white line energy between arsenic sulfide species, resolving specific phases is more challenging. To overcome this limitation, we utilized variation in the EXAFS (χ) spectra between phases; analysis of the k^3-weighted As χ function to a k of 15.5 $Å^{-1}$ shows the chemical form of arsenic in the bulk peat sample conforms to that of arsenian pyrite (Fig. 3a). Other As sulfides, including arsenopyrite, realgar, and orpiment, as well as organic arsenic species were not observed (Fig. A.8). The first and second peak positions in the Fourier transformation of the $\chi(k)$ for arsenian pyrite and peat are aligned (Fig. 3b). Further, arsenian pyrite accounts for every oscillation in the real part of the Fourier transformation of the peat's $\chi(k)$ (Fig. 3c). The amplitude of the $\chi(k)$ and the magnitude of Fourier transformation are quenched for the peat relative to the arsenian pyrite standard, likely reflecting a lower crystallinity in the peat.

Solid-phase As is heterogeneously distributed in the peat (Fig. 4), concentrating on the exterior of individual peat grains and co-associating with S and Fe (Fig. 4b). Additionally, S is present in areas of the peat where As is not, and Fe is common throughout the peat. We chose prominent grains depicted in Fig. 4 to illustrate the speciation of As (Fig. 5) and its association with Fe (Figs. 6 and 7) and S (Figs. 8 and 10). Within the peat grains depicted in Fig. 5a, As resides as a combination of As-bearing sulfides and as arsenite (adsorbed), ranging from 72 to 100 % As-sulfide (Table A.2). Further, within the grains in Fig. 5b, As is comprised of As-bearing sulfides and arsenite, ranging from 81 to 100 % As-sulfide (Table A.2). The multiple energy mapping and μXANES fitting routine

corroborate the As speciation observed from the individual μXANES spectra, with As-bearing sulfides dominating the grain-As speciation and arsenite making a minor contribution (Fig. A.7).

3.5. Solid-phase iron speciation in peat.

Solid-phase Fe concentration is highest around the exterior of the individual peat grains and in general parallels the spatial distribution of As (Figs. 5 and 6). Iron(II) predominates in the areas of highest Fe (and As) concentration based on μXANES analysis (Fig. 6; Table A.3). The Fe hotspot associated with the As-bearing sulfide is exclusively Fe(II). In general, Fe(II) is higher where iron (and arsenic) are concentrated, whereas the proportion of Fe(III) increases in regions of low Fe concentration (Fig. 6c). Least squares fitting of the Fe EXAFS function of the bulk peat sample confirms the presence of pyrite (27 %), Fe (hydr)oxides (hematite and goethite) (14 %), and Fe-bearing silicates (clinochlore and ferruginous smectite) (62 %) (Fig. 7).

3.6. Solid-phase sulfur speciation in peat.

The solid-phase distribution of S in the peat grains coincides with that of As and Fe; high S concentrations are found along the grain exterior (Fig. 8). Principal component analysis of the multiple energy maps coupled with S μXANES spectral analysis shows complex S speciation (Figs. 9 and 10). Sulfur μXANES spectra of the peat grains indicate a predominance of pyrite on the grain

exterior that grades to organic S species (i.e., organic sulfides, sulfoxides, and sulfate esters) in the interior (Figs. 10 and A.4; Table A.1), corroborating the bulk S XANES spectrum comprised of pyrite and organic S species (Figs. 8c and A.5).

4. DISCUSSION

4.1. Authigenic arsenian pyrite formation

Our site transitioned from a salt marsh to mangrove forest containing brackish water between 8.5 to 6.3 cal ka BP owing to sea level rise accompanying sediment aggradation and delta progradation, producing peat layers throughout the surrounding upper Mekong Delta (Nguyen et al., 2005; Tamura et al., 2009). The peat at 6 m depth in our site, aged 5.675 ± 0.020 ka, which directly underlies gray sediments representative of a flood plain depositional environment, likely corresponds to the "organic mud" of similar depth in sediment cores collected proximal to our field site (Tamura et al., 2009). Thus, the peat developed in a saline environment that likely continued even as the coastline receded southeast to present-day Vietnam, as saltwater intrusion may have occurred up to tens of kilometers along the Mekong during high tide in the dry season – the extent of present-day seawater intrusion (Hori, 2000; Tamura et al., 2007). Seawater likely assisted in supplying the necessary sulfur (sulfate) for arsenian pyrite formation. Even with low sulfate reduction rates, a low sedimentation rate of ~ 0.3 m/ka from ~ 5.7 ka to 3.8 ka at our site (Electronic Annex), arsenian pyrite formation would result in anoxic, H_2S-poor and reactive iron-rich peat (Huertadiaz and Morse, 1992). The reactivity of the organic matter was likely sufficient to fuel sulfate reduction for a period of time after deposition as in other marine environments (Huertadiaz

and Morse, 1992; Morse and Wang, 1997). The iron supply likely came from iron (hydr)oxides and weathering of primary silicate minerals (Fig. 7) (Lowers et al., 2007; Morse and Wang, 1997; Poulton et al., 2004).

Microscale X-ray imaging and spectroscopy reveals that arsenian pyrite exists as coatings on peat grain exteriors (Figs. 4 – 6 and A.7). Arsenic and sulfur enrichment on grain exteriors (Figs. 4 – 5 and 8 – 10) suggests supply through an aqueous source with precipitation on the organic (peat) particle. Additionally, the lack of correlation between arsenic or sulfur and the concentrations of the chalcophiles copper and zinc implies authigenic origin; R^2 values are ≤ 0.006 (n = 147,568) for the linear regressions of As vs. Cu, As vs. Zn, S vs. Cu, and S vs. Zn (data not shown). In contrast, clastic pyrite grains often retain chalcophile correlations reflective of the pyritic source material (Leblanc et al., 2000). Finally, SEM/electron microprobe shows framboidal pyrite (data not shown) consistent with authigenic formation (Lowers et al., 2007; Nickson et al., 2000).

Arsenic speciation on the grain exteriors is a combination of As sulfide (predominantly arsenian pyrite) and arsenite (Fig. 5). The adsorbed arsenite may result from inadequate sulfur supply from infiltrating surface water and/or peat decomposition; alternatively, it may have formed through a progressive loss of S with infiltrating waters of freshwater origin. The coexistence of iron (hydr)oxides and pyrite in the peat (Fig. 7) and the close association of Fe(II) and Fe(III) minerals in general (Fig. 6) indicate the potential for iron transformation reactions, which may be kinetically hindered under anoxic conditions (Wersin et al., 1991) and/or limited by pore-water diffusion within peat grains/aggregates.

Because the net annual water flux through the ~ 15 m surface clay aquitard of our field site is vertical (Benner et al., 2008; Polizzotto et al., 2008), we can use the trend in pore-water arsenic concentrations along the flow path to evaluate whether the peat layer is currently acting as a source or a sink. The aqueous arsenic concentrations are not significantly different above (measured at ~ 3 m depth), within (measured at ~ 6 m depth), or below (measured at ~ 8 m) the peat (Fig. A.9), indicating there is currently no detectable As mass transfer to or from the peat. If pyritization were currently occurring in the peat, we would expect the aqueous arsenic concentration to be lower in the peat relative to the overlying strata. The aqueous arsenic profile along with low dissolved sulfide concentrations (median = 13 nM in shallow wells in our field area (Kocar et al., 2008)) suggest sulfidization and pyritization in the peat are not currently dominant processes controlling vertically transported dissolved arsenic. Nevertheless, low levels of sulfidogenesis may persist in the presence of Fe(II) and/or Fe(III), which can scavenge sulfide from pore-water. Nevertheless, the low dissolved sulfide limits the extent of potential pyrite formation through heterogeneous nucleation on iron-rich clays without a $FeS_{(s)}$ precursor (Lowers et al., 2007; Rickard et al., 2007). Further, $FeS_{(s)}$ is undersaturated with respect to Fe^{2+} and HS^- in the peat (assuming pH = 7.4, $Fe^{2+} = 2.2 \pm 0.9 \times 10^{-4}$ M, $HS^- = 30$ nM, and $\log K_{sp} = -3$ (Lindsay, 1979), the saturation index = -2.8), and is not detected in the peat by Fe EXAFS (Fig. 7), S XANES (Fig. 8), or XRD (Fig. A.3). Thus, the current geochemical conditions in the peat do not favor pyrite formation, which requires $FeS_{(s)}$ and/or greigite (Fe_3S_4) – also not detected – as a precursor (Rickard, 1997; Rickard and Luther, 1997; Schoonen, 2004; Wilkin and Barnes, 1997). Pyritization in the peat is thus likely a remnant of past sulfate reducing conditions.

4.2. Arsenic speciation and retention.

Arsenian pyrite is stable under anoxic conditions (Schoonen, 2004), helping to explain the low dissolved arsenic concentration in the peat (Fig. 2). Anoxic conditions in the peat were noted by signatures of methanogensis and metal reduction, along with redoximorphic features. As in other organic-rich freshwater and marine sediments (Huertadiaz et al., 1993; Huertadiaz and Morse, 1992), the peat deposit studied here, being of estuarine/marine origin, would provide the sulfur and nucleation sites for pyrite formation and growth. A high organic carbon concentration promotes the formation – and actually the persistence of – iron sulfides in sediments (Morgan et al., 2012; Morse and Wang, 1997). A slowing of iron monosulfides-to-pyrite transformation kinetics through passivation by DOC or As(III) may occur over decadal timescales (Wilkin and Ford, 2006), allowing more time for arsenic to co-precipitate with the pyrite – the predominant host of co-precipitated As and the most stable among iron sulfides (Kirk et al., 2010). Arsenic is incorporated into the crystal lattice of arsenian pyrite (Savage et al., 2000), consistent with the observation of pyrite by iron and sulfur XAS (Figs. 7 and 8) and sediments of the Bengal Basin and the Pearl River Delta (China) (Lowers et al., 2007; Wang et al., 2012).

Though arsenian pyrite is the principal As mineral in the peat layer here (which is of estuarine origin), alternate arsenic sulfides (lacking iron) may predominate in other estuarine sediment systems. For instance, incubation of fresh sediment from a temperate estuarine salt marsh with 55 uM As(III) leads to the formation of orpiment after initially adsorbing onto pyrite (Bostick et

al., 2004), in contrast to our site, which has a lower total aqueous arsenic concentration (0.57 ± 0.14 uM As). In shallow, reducing aquifer sediments adjacent to the San Francisco Bay, CA, realgar is the dominant As-bearing sulfide present with no evidence for coprecipitation of arsenic with pyrite (O'Day et al., 2004). Total solid-phase arsenic levels are in the same range (1 – 3 mmol As kg^{-1}) as the peat studied here, though the aqueous concentrations are much higher in some areas (< 0.07 to 200 uM As) and the H_2S activity is buffered by iron sulfide and iron (hydr)oxides at circumneutral pH (O'Day et al., 2004).

Apart from the precipitation of sulfide minerals, organically bound arsenic is another means of As retention in peat. For example, in a groundwater-fed wetland enriched in arsenic from the weathering and erosion of As-bearing sulfide ore deposits, As is predominantly bound to sulfur groups of peat under persistent anoxic conditions (depth ~ 1.5 – 2.5 m), and to realgar in non-equilibrium conditions at the surface (depth ~ 0 to 0.4 m) (Langner et al., 2012; Langner et al., 2013); arsenopyrite and arsenian pyrite are only minor arsenic species (Langner et al., 2013). The Swiss peatland samples examined by Langner et al. (2012) have higher S/Fe ratios (> 2 in depths ~ 1.5 – 2.5 m, sites B1 and B6) and much lower Fe/As ratios (< 50 in depths ~ 0 to 0.4 m, sites B3 and B5) than those found in the Cambodian Mekong Delta of 0.6 and 438, respectively. Flow-through reactors running influent solutions containing 20 mM As and 200 mM SO_4^{2-} through freshwater lake-bottom sediments for an 8-week period similarly sequestered As and S through the formation of $AsS_{(s)}$ and thiol-bound As(III) (Couture et al., 2013b). The influent concentration of 20 mM As is 2 orders of magnitude higher than current (and likely past) pore-water As levels in our sediment profile (Fig. A.9), improving the potential for $AsS_{(s)}$ precipitation. In contrast to freshwater systems, sulfurization of organic matter in marine systems occurs more slowly than iron

sulfide formation (on the order of 10^2 – 10^4 years) (Werne et al., 2004). Though organic sulfur species are evident in both the bulk S XANES (Fig. 8) and S μXANES spectra (Fig. 10) of our peat, organic sulfur-bound As is not detected (Figs. 3 and A.8). Thus, organic matter sulfurization evidently did not compete with pyritization under the estuarine conditions of peat deposition here.

4.3. Mass balance for arsenic enrichment in peat

The total arsenic concentration in the peat is 153 mg As kg^{-1} (Table 1). Compared to the mean concentration in the 6 m of sediment above the peat (15.8 ± 4.7 mg As kg^{-1}), the apparent enrichment is approximately 10-fold above the baseline level. Pore-water arsenic concentrations suggest that As sequestration in the peat layer is not operative presently, and we posit that the dominant loading of arsenic occurred during the reducing and residually saline conditions during and following peat deposition, which commenced some 5.7 ka BP. Aqueous arsenic supply to the peat would occur through the reductive dissolution of As/Fe-bearing solids annually delivered to the site in overlying sediment. Geochemical analysis of the sediment profile allows us to approximate the period over which the observed level of arsenic enrichment would occur. Assuming a reductive dissolution rate of annually deposited Himalayan sediment estimated previously for our field area (Polizzotto et al., 2008) and a calculated sediment accumulation rate from ^{14}C dating, the noted arsenic levels in the peat layer would be achieved within 1800 years (estimates of the temporal period for enrichment are provided within the Electronic Annex).

4.4. Arsenic reactivity

Despite a ten-fold increase in total As concentration in the peat layer relative to the overlying sediment, the acid-extractable fraction remained constant at 1 – 2 mg As kg^{-1} throughout the profile (Fig. 1). Bulk As EXAFS indicates arsenic is predominantly arsenian pyrite (Fig. 3), and consistent with expectations, citrate-bicarbonate-dithionite extraction released only 1 % of the total arsenic in the peat (data not shown). Thus, iron (hydr)oxides (e.g., hematite) do not host appreciable arsenic within these high-As zones, and reductive dissolution is not a release mechanism. Though the total abundance of carbon (21.5 % w/w – principally in organic form) might suggest the peat would have the electron donating capacity to facilitate microbial-driven dissimilatory iron and/or arsenic reduction, incubation of the peat with As-goethite did not lead to arsenic release; it, in fact, decreased release presumably owing to an increased adsorbent concentration (Fig. 2). Therefore, microbial utilization of organic carbon within the peat is prohibitive for driving iron (hydr)oxides reductive dissolution (at least on short timescales). Further, arsenic in the peat is already present in a reduced form, precluding direct As(V) reduction as a release mechanism. Hence, arsenic in the peat is in a form that is immune to anaerobic microbially driven release mechanisms.

5. SUMMARY and CONCLUSIONS

Buried peat formed under saline conditions is common through much of the Mekong Delta, and therefore likely hosts a concentrated zone of arsenic in near-surface sediments. A ~ 6.3 to 6.5 ka mangrove peat layer over 5 m thick extends through a large portion of Mekong River lowland, from Phnom Penh to the Vietnam border (Tamura et al., 2009). Similarly, mangrove peat of 6.0 to 6.5 ka is found in the innermost part of the Mekong Delta in Vietnam (Nguyen et al., 2005).

In this study, peat formed during delta formation provided the biogeochemical requirements for the formation of arsenian pyrite – a chemically stable form under anoxic conditions – that led to arsenic enrichment relative to overlying sediment. The arsenic supply in the buried peat-rich sediment results from reductive dissolution of As-bearing iron (hydr)oxides around the time of burial and/or subsequent advective transport of As released in overlying sediment (Polizzotto et al., 2008). Arsenic is not currently associated with iron (hydr)oxides in the peat, and therefore is not subject to release by reductive dissolution. The organic carbon in the peat studied here, coupled with its microbial community, does not lead to reductive dissolution of exogenous arsenic-bearing iron (hydr)oxides (Fig. 2). Further, the peat layer does not appear to be sequestering nor liberating arsenic currently based on pore-water concentration profiles. Nevertheless, we do not suggest the arsenian pyrite is in equilibrium with the sediment pore-water; rather, the extent to which arsenian pyrite is currently forming or dissolving is below our ability to detect here. We suggest that buried peat in the Mekong Delta and in analogous deltas worldwide, such as the Bengal Basin, served as a sink for arsenic under conditions of formation, presently host an enrichment of As, and would be a detectable source of As to pore-water only if the arsenian pyrite were oxidized.

Anthropogenic and climate-induced perturbations could increase the potential for oxidation of arsenian pyrite in near-surface peat layers. For instance, drawdown from increasing groundwater exploitation of the Mekong Delta could promote oxygen penetration deeper into the sediment profile and oxidize arsenian pyrite in peat layers. Alternatively, excavation of near-surface clayey sediments for brick making – a common practice in the Mekong Delta – can expose buried peat layers to oxygen. Finally, projected increases in land surface temperature may promote increased rates of organic matter degradation in soils/sediments, thereby destabilizing buried peat layers.

ACKNOWLEDGEMENTS

This work was funded by a US EPA STAR Graduate Fellowship awarded to J.W. Stuckey, the Stanford Woods Institute for the Environment, and a National Science Foundation Graduate Research Fellowship Program Grant no. DGE-114747 awarded to M.V. Schaefer. Portions of this work were also supported by the National Science Foundation (grant number EAR-0952019), the Stanford NSF Environmental Molecular Science Institute (NSF-CHE-0431425), and the EVP program of Stanford's Woods Institute.

We are indebted to the staff at Resource Development International for logistical and field support, including Andrew Shantz, Thang Makara, Kuy Dina, and Phen Nuon. We are grateful to Guangchao Li, Simon Wang, Max Guillaume, Kristin Boye, and Sarah McCurdy for laboratory assistance, and Debra Hausladen and Angelia Seyfferth for help with fieldwork. We thank Ruben Kretzschmar and Kurt Barmettler for access to the XRF at ETH Zurich. We would like to thank Sam Webb for assistance in XRF/XAS data collection. Finally, we would like to thank three anonymous reviewers and the Associated Editor for their helpful comments to improve this manuscript. Use of the Stanford Synchrotron Radiation Lightsource, SLAC National Accelerator Laboratory, is supported by the U.S. Department of Energy, Office of Science, Office of Basic Energy Sciences under Contract No. DE-AC02-76SF00515.

REFERENCES

Ahmed, M.F., Ahuja, S., Alauddin, M., Hug, S.J., Lloyd, J.R., Pfaff, A., Pichler, T., Saltikov, C., Stute, M. and van Geen, A. (2006) Epidemiology - ensuring safe drinking water in Bangladesh. *Science* **314**, 1687-1688.

Akai, J., Izumi, K., Fukuhara, H., Masuda, H., Nakano, S., Yoshimura, T., Ohfuji, H., Anawar, H.M. and Akai, K. (2004) Mineralogical and geomicrobiological investigations on groundwater arsenic enrichment in Bangladesh. *Appl. Geochem.* **19**, 215-230.

Almkvist, G., Boye, K. and Persson, I. (2010) K-edge XANES analysis of sulfur compounds: an investigation of the relative intensities using internal calibration. *J. Synchrotron Radiat.* **17**, 683-688.

Benner, S.G., Polizzotto, M.L., Kocar, B.D., Ganguly, S., Phan, K., Ouch, K., Sampson, M. and Fendorf, S. (2008) Groundwater flow in an arsenic-contaminated aquifer, Mekong Delta, Cambodia. *Appl. Geochem.* **23**, 3072-3087.

Berg, M., Stengel, C., Trang, P.T.K., Viet, P.H., Sampson, M.L., Leng, M., Samreth, S. and Fredericks, D. (2007) Magnitude of arsenic pollution in the Mekong and Red River Deltas - Cambodia and Vietnam. *Sci. Total Environ.* **372**, 413-425.

Bostick, B.C., Chen, C. and Fendorf, S. (2004) Arsenite retention mechanisms within estuarine sediments of Pescadero, CA. *Environ. Sci. Technol.* **38**, 3299-3304.

Bostick, B.C. and Fendorf, S. (2003) Arsenite sorption on troilite (FeS) and pyrite (FeS2). *Geochim. Cosmochim. Acta* **67**, 909-921.

Buschmann, J. and Berg, M. (2009) Impact of sulfate reduction on the scale of arsenic contamination in groundwater of the Mekong, Bengal and Red River deltas. *Appl. Geochem.* **24**, 1278-1286.

Chatterjee, A., Das, D., Mandal, B.K., Chowdhury, T.R., Samanta, G. and Chakraborti, D. (1995) Arsenic in ground-water in 6 districts of West-Bengal, India - the biggest arsenic calamity in the world .1. Arsenic species in drinking-water and urine of the affected people. *Analyst* **120**, 643-650.

Couture, R.-M., Gobeil, C. and Tessier, A. (2010) Arsenic, iron and sulfur co-diagenesis in lake sediments. *Geochim. Cosmochim. Acta* **74**, 1238-1255.

Couture, R.M., Rose, J., Kumar, N., Mitchell, K., Wallschlager, D. and Van Cappellen, P. (2013a) Sorption of Arsenite, Arsenate, and Thioarsenates to Iron Oxides and Iron Sulfides: A Kinetic and Spectroscopic Investigation. *Environ. Sci. Technol.* **47**, 5652-5659.

Couture, R.M., Wallschlager, D., Rose, J. and Van Cappellen, P. (2013b) Arsenic binding to organic and inorganic sulfur species during microbial sulfate reduction: a sediment flow-through reactor experiment. *Environ. Chem.* **10**, 285-294.

Dittmar, J., Voegelin, A., Roberts, L.C., Hug, S.J., Saha, G.C., Ali, M.A., Badruzzaman, A.B.M. and Kretzschmar, R. (2007) Spatial distribution and temporal variability of arsenic in irrigated rice fields in Bangladesh. 2. Paddy soil. *Environ. Sci. Technol.* **41**, 5967-5972.

Dixit, S. and Hering, J.G. (2003) Comparison of arsenic(V) and arsenic(III) sorption onto iron oxide minerals: implications for arsenic mobility. *Environ. Sci. Technol.* **37**, 4182-4189.

Fendorf, S. and Kocar, B.D. (2009) Biogeochemical processes controlling the fate and transport of arsenic: implications for South and Southeast Asia, *Adv. Agron*. **104**, pp. 137-164.

Fleet, M., MacLean, P. and Barbier, J. (1989) Oscillatory-zoned As-bearing pyrite from strata-bound and stratiform gold deposits: an indicator of ore fluid evolution. *Econ. Geol. Mg.* **6**, 356-362.

Hori, H. (2000) *The Mekong: environment and development.* United Nations University Press, Tokyo.

Huertadiaz, M.A., Carignan, R. and Tessier, A. (1993) Measurement of trace-metals associated with acid volatile sulfides and pyrite in organic fresh-water sediments. *Environ. Sci. Technol.* **27**, 2367-2372.

Huertadiaz, M.A. and Morse, J.W. (1992) Pyritization of trace-metals in anoxic marine-sediments. *Geochim Cosmochim. Acta* **56**, 2681-2702.

Islam, F.S., Gault, A.G., Boothman, C., Polya, D.A., Charnock, J.M., Chatterjee, D. and Lloyd, J.R. (2004) Role of metal-reducing bacteria in arsenic release from Bengal delta sediments. *Nature* **430**, 68-71.

Keon, N.E., Swartz, C.H., Brabander, D.J., Harvey, C.F. and Hemond, H.F. (2001) Validation of an arsenic sequential extraction method for evaluating mobility in sediments. *Environ. Sci. Technol.* **35**, 2778-2784.

Kirk, M.F., Roden, E.E., Crossey, L.J., Brearley, A.J. and Spilde, M.N. (2010) Experimental analysis of arsenic precipitation during microbial sulfate and iron reduction in model aquifer sediment reactors. *Geochim. Cosmochim. Acta* **74**, 2538-2555.

Kocar, B.D. and Fendorf, S. (2009) Thermodynamic constraints on reductive reactions influencing the biogeochemistry of arsenic in soils and sediments. *Environ. Sci. Technol.* **43**, 4871-4877.

Kocar, B.D., Polizzotto, M.L., Benner, S.G., Ying, S.C., Ung, M., Ouch, K., Samreth, S., Suy, B., Phan, K., Sampson, M. and Fendorf, S. (2008) Integrated biogeochemical and hydrologic processes driving arsenic release from shallow sediments to groundwaters of the Mekong delta. *Appl. Geochem.* **23**, 3059-3071.

Langner, P., Mikutta, C. and Kretzschmar, R. (2012) Arsenic sequestration by organic sulphur in peat. *Nat. Geosci.* **5**, 66-73.

Langner, P., Mikutta, C., Suess, E., Marcus, M.A. and Kretzschmar, R. (2013) Spatial distribution and speciation of arsenic in peat studied with microfocused x-ray fluorescence spectrometry and x-ray absorption spectroscopy. *Environ. Sci. Technol.* **47**, 9706-9714.

Leblanc, M., Morales, J.A., Borrego, J. and Elbaz-Poulichet, F. (2000) 4,500-year-old mining pollution in southwestern Spain: Long-term implications for modern mining pollution. *Econ. Geol. Bull. Soc.* **95**, 655-661.

Lindsay, W.L. (1979) *Chemical equilibria in soils.* John Wiley & Sons, New York.

Loeppert, R.H. and Inskeep, W.P. (1996) Iron, in: Bigham, J.M. (Ed.), *Methods of Soil Analysis.* Soil Science Society of America, Inc., Madison, pp. 639-664.

Lowers, H.A., Breit, G.N., Foster, A.L., Whitney, J., Yount, J., Uddin, N. and Muneem, A. (2007) Arsenic incorporation into authigenic pyrite, bengal basin sediment, Bangladesh. *Geochim. Cosmochim. Acta* **71**, 2699-2717.

Mayhew, L.E., Webb, S.M. and Templeton, A.S. (2011) Microscale imaging and identification of Fe speciation and distribution during fluid-mineral reactions under highly reducing conditions. *Environ. Sci. Technol.* **45**, 4468-4474.

McArthur, J.M., Banerjee, D.M., Hudson-Edwards, K.A., Mishra, R., Purohit, R., Ravenscroft, P., Cronin, A., Howarth, R.J., Chatterjee, A., Talukder, T., Lowry, D., Houghton, S. and Chadha, D.K. (2004) Natural organic matter in sedimentary basins and its relation to arsenic in anoxic ground water: the example of West Bengal and its worldwide implications. *Appl. Geochem.* **19**, 1255-1293.

McArthur, J.M., Banerjee, D.M., Sengupta, S., Ravenscroft, P., Klump, S., Sarkar, A., Disch, B. and Kipfer, R. (2010) Migration of As, and H-3/(3) He ages, in groundwater from West Bengal: implications for monitoring. *Water Res.* **44**, 4171-4185.

McArthur, J.M., Nath, B., Banerjee, D.M., Purohit, R. and Grassineau, N. (2011) Palaeosol control on groundwater flow and pollutant distribution: the example of arsenic. *Environ. Sci. Technol.* **45**, 1376-1383.

McArthur, J.M., Ravenscroft, P., Banerjee, D.M., Milsom, J., Hudson-Edwards, K.A., Sengupta, S., Bristow, C., Sarkar, A., Tonkin, S. and Purohit, R. (2008) How paleosols influence groundwater flow and arsenic pollution: a model from the Bengal Basin and its worldwide implication. *Water Resour. Res.* **44**, W11411, doi:10.1029/2007WR006552.

McArthur, J.M., Ravenscroft, P., Safiulla, S. and Thirlwall, M.F. (2001) Arsenic in groundwater: testing pollution mechanisms for sedimentary aquifers in Bangladesh. *Water Resour. Res.* **37**, 109-117.

Morgan, B., Burton, E.D. and Rate, A.W. (2012) Iron monosulfide enrichment and the presence of organosulfur in eutrophic estuarine sediments. *Chem. Geol.* **296**, 119-130.

Morse, J.W. and Rickard, D. (2004) Chemical dynamics of sedimentary acid volatile sulfide. *Environ. Sci. Technol.* **38**, 131A-136A.

Morse, J.W. and Wang, Q.W. (1997) Pyrite formation under conditions approximating those in anoxic sediments .2. Influence of precursor iron minerals and organic matter. *Mar. Chem.* **57**, 187-193.

Nguyen, V.L., Ta, T.K.O., Tateishi, M., Kobayashi, I. and Saito, Y. (2005) Holocene evolution of the Mekong river delta, Vietnam. *J. Geol. Soc. Japan* **111**, XXI.

Nickson, R., McArthur, J., Burgess, W., Ahmed, K.M., Ravenscroft, P. and Rahman, M. (1998) Arsenic poisoning of Bangladesh groundwater. *Nature* **395**, 338-338.

Nickson, R.T., McArthur, J.M., Ravenscroft, P., Burgess, W.G. and Ahmed, K.M. (2000) Mechanism of arsenic release to groundwater, Bangladesh and West Bengal. *Appl. Geochem.* **15**, 403-413.

O'Day, P.A., Vlassopoulos, D., Root, R. and Rivera, N. (2004) The influence of sulfur and iron on dissolved arsenic concentrations in the shallow subsurface under changing redox conditions. *P. Natl. Acad. Sci. USA* **101**, 13703-13708.

Polizzotto, M.L., Harvey, C.F., Sutton, S.R. and Fendorf, S. (2005) Processes conducive to the release and transport of arsenic into aquifers of Bangladesh. *P. Natl. Acad. Sci. USA* **102**, 18819-18823.

Polizzotto, M.L., Kocar, B.D., Benner, S.G., Sampson, M. and Fendorf, S. (2008) Near-surface wetland sediments as a source of arsenic release to ground water in Asia. *Nature* **454**, 505-U505.

Postma, D. and Jakobsen, R. (1996) Redox zonation: equilibrium constraints on the Fe(III)/SO4-reduction interface. *Geochim. Cosmochim. Acta* **60**, 3169-3175.

Postma, D., Larsen, F., Hue, N.T.M., Duc, M.T., Viet, P.H., Nhan, P.Q. and Jessen, S. (2007) Arsenic in groundwater of the Red River floodplain, Vietnam: controlling geochemical processes and reactive transport modeling. *Geochim. Cosmochim. Acta* **71**, 5054-5071.

Poulton, S.W., Krom, M.D. and Raiswell, R. (2004) A revised scheme for the reactivity of iron (oxyhydr)oxide minerals towards dissolved sulfide. *Geochim. Cosmochim. Acta* **68**, 3703-3715.

Ravel, B. and Newville, M. (2005) Athena, Artemis, Hephaestus: data analysis for X-ray absorption spectroscopy using IFEFFIT. *J. Synchrotron Radiat.* **12**, 537-541.

Ravenscroft, P., Brammer, H. and Richards, K. (2009) *Arsenic pollution: a global synthesis.* Wiley-Blackwell, Chichester, UK.

Rickard, D. (1997) Kinetics of pyrite formation by the H2S oxidation of iron (II) monosulfide in aqueous solutions between 25 and 125 degrees C: the rate equation. *Geochim. Cosmochim. Acta* **61**, 115-134.

Rickard, D., Grimes, S., Butler, I., Oldroyd, A. and Davies, K.L. (2007) Botanical constraints on pyrite formation. *Chem. Geol.* **236**, 228-246.

Rickard, D. and Luther, G.W. (1997) Kinetics of pyrite formation by the H2S oxidation of iron(II) monosulfide in aqueous solutions between 25 and 125 degrees C: the mechanism. *Geochim. Cosmochim. Acta* **61**, 135-147.

Rickard, D.T. (1975) Kinetics and mechanism of pyrite formation at low-temperatures. *Am. J. Sci.* **275**, 636-652.

Sambu, S. and Wilson, R. (2008) Arsenic in food and water - a brief history. *Toxicol. Ind. Health* **24**, 217-226.

Saunders, J.A., Lee, M.K., Uddin, A., Mohammad, S., Wilkin, R.T., Fayek, M. and Korte, N.E. (2005) Natural arsenic contamination of Holocene alluvial aquifers by linked tectonic, weathering, and microbial processes. *Geochem. Geophy. Geosy.* **6**, Q04006, doi:*10.1029/2004GC000803*.

Savage, K.S., Tingle, T.N., O'Day, P.A., Waychunas, G.A. and Bird, D.K. (2000) Arsenic speciation in pyrite and secondary weathering phases, Mother Lode Gold District, Tuolumne County, California. *Appl. Geochem.* **15**, 1219-1244.

Schoonen, M.A.A. (2004) Mechanisms of sedimentary pyrite formation, in: Amend, J.P., Edwards, K.J., Lyons, T.W. (Eds.), *Sulfur biogeochemistry - past and present.* Geological Society of America, pp. 117-134.

Schwertmann, U. and Cornell, R.M. (2000) *Iron oxides in the laboratory*, Second, Completely Revised and Extended ed. Wiley-VCH, Weinheim, Federal Republic of Germany.

Smedley, P.L. and Kinniburgh, D.G. (2002) A review of the source, behaviour and distribution of arsenic in natural waters. *Appl. Geochem.* **17**, 517-568.

Tamura, T., Saito, Y., Sieng, S., Ben, B., Kong, M., Choup, S. and Tsukawaki, S. (2007) Depositional facies and radiocarbon ages of a drill core from the Mekong River lowland near Phnom Penh, Cambodia: evidence for tidal sedimentation at the time of Holocene maximum flooding. *J. Asian Earth Sci.* **29**, 585-592.

Tamura, T., Saito, Y., Sieng, S., Ben, B., Kong, M., Sim, I., Choup, S. and Akiba, F. (2009) Initiation of the Mekong River delta at 8 ka: evidence from the sedimentary succession in the Cambodian lowland. *Quaternary Sci. Rev. Special Theme: Modern Analogues in Quaternary Palaeoglaciological Reconstruction* (pp. 181-260) **28**, 327-344.

Tufano, K.J., Reyes, C., Saltikov, C.W. and Fendorf, S. (2008) Reductive processes controlling arsenic retention: revealing the relative importance of iron and arsenic reduction. *Environ. Sci. Technol.* **42**, 8283-8289.

Van Geen, A., Rose, J., Thoral, S., Garnier, J.M., Zheng, Y. and Bottero, J.Y. (2004) Decoupling of As and Fe release to Bangladesh groundwater under reducing conditions. Part II: Evidence from sediment incubations. *Geochim. Cosmochim. Acta* **68**, 3475-3486.

Wang, Y., Jiao, J.J. and Cherry, J.A. (2012) Occurrence and geochemical behavior of arsenic in a coastal aquifer-aquitard system of the Pearl River Delta, China. *Sci. Total Environ.* **427**, 286-297.

Webb, S.M. (2005) SIXpack: a graphical user interface for XAS analysis using IFEFFIT. *Phys. Scripta* **T115**, 1011-1014.

Webb, S.M. (2011) The microanalysis toolkit: x-ray fluorescence image processing software, in: McNulty, I., Eyberger, C., Lai, B. (Eds.), *10th International Conference on X-Ray Microscopy*, pp. 196-199.

Werne, J.P., Hollander, D.J., Lyons, T.W. and Damsté, J.S. (2004) Organic sulfur biogeochemistry: recent advances and future research directions. *Geol. S. Am. S.*, 135-150.

Wersin, P., Hohener, P., Giovanoli, R. and Stumm, W. (1991) Early diagenetic influences on iron transformations in a fresh-water lake sediment. *Chem. Geol.* **90**, 233-252.

Wilkin, R. and Barnes, H. (1997) Formation processes of framboidal pyrite. *Geochim. Cosmochim. Acta* **61**, 323-339.

Wilkin, R.T. and Ford, R.G. (2006) Arsenic solid-phase partitioning in reducing sediments of a contaminated wetland. *Chem. Geol.* **228**, 156-174.

Yu, W.H., Harvey, C.M. and Harvey, C.F. (2003) Arsenic in groundwater in Bangladesh: a geostatistical and epidemiological framework for evaluating health effects and potential remedies. *Water Resour. Res.* **39**, 1146, doi:*10.1029/2002WR001327*, *6*.

Tables

Table 1. Elemental composition of the sediment profile of a seasonally flooded wetland to a depth of 6 m.

Depth	pH[a]	N		C		C/N		Si	Al	Fe	Ti	Mn	Cu	Zn	As	S	P
(m)		Mean (g/kg)	SD (g/kg)	Mean (g/kg)	SD (g/kg)	Mean	SD	(g/kg)	(g/kg)	(g/kg)	(g/kg)	(µg/g)	(µg/g)	(µg/g)	(µg/g)	(µg/g)	(µg/g)
0.26	5.3	0.52	0.02	5.37	0.08	10.3	0.4	228	77	48	5.0	426	34	103	16	140	447
0.46	5.8	0.43	0.02	5.05	0.03	11.8	0.6	221	79	47	5.1	712	37	102	17	96	454
0.66	6.1	0.41	0.01	4.38	0.01	10.6	0.3	227	79	49	5.2	563	35	99	18	119	520
0.86	6.2	0.34	0.00	4.02	0.01	11.8	0.1	229	77	44	5.3	395	37	99	14	103	477
1.06	6.4	0.38	0.03	4.49	0.03	11.7	0.9	222	80	50	5.3	761	39	101	20	247	508
1.26	6.5	0.37	0.01	3.85	0.03	10.4	0.3	222	80	50	5.2	811	38	104	19	145	493
1.46	6.6	0.37	0.04	3.93	0.02	10.6	1.0	228	76	50	5.3	716	36	101	24	149	554
1.66	6.5	0.33	0.01	3.87	0.01	11.8	0.5	223	78	51	5.3	594	38	102	21	135	534
1.80	6.5	0.34	0.03	3.70	0.04	10.9	1.1	221	80	48	5.2	559	42	102	18	114	484
2.20	6.7	0.41	0.00	3.00	0.00	7.2	0.1	211	85	43	4.8	271	36	110	12	121	266
2.63	6.8	0.29	0.02	2.45	0.03	8.3	0.7	232	80	40	5.0	423	35	105	10	89	286
3.70	6.8	0.49	0.01	4.92	0.02	10.1	0.3	203	87	39	4.5	312	39	112	12	213	186
4.20	6.6	0.28	0.03	2.94	0.06	10.5	1.0	206	76	52	5.2	314	38	101	16	2346	291
4.60	6.8	0.28	0.03	2.76	0.02	9.9	0.9	220	81	43	5.3	349	35	103	12	863	279
5.00	6.6	0.92	0.03	7.88	0.06	8.5	0.3	188	94	42	4.1	328	55	114	13	366	105
5.46	6.2	1.60	0.03	17.14	0.05	10.7	0.2	187	97	32	3.9	214	74	124	14	555	173
5.55	4.3	3.36	0.02	54.44	0.71	16.2	0.2	172	87	29	3.5	328	72	109	25	5265	170
5.80	5.4	0.63	0.02	8.48	1.46	13.4	2.3	231	90	24	5.7	184	40	101	10	432	216
6.10	3.1	3.19	0.02	214.57	17.65	67.2	5.5	149	54	50	3.3	754	41	127	153	15920	477

[a]Sediment pH was measured in 0.01 M $CaCl_2$.

Table 2. Sediment age determined by radiocarbon dating.

Depth (m)	δ13C (‰)[a]	Δ14C (‰)[b]	14C Age (BP)[c]
0.46	-19.36	-115.8	930
0.86	-21.28	-154.7	1290
1.26	-22.15	-185.4	1590
1.66	-23.25	-176.8	1505
2.63	-24.07	-258.5	2345
3.70	-23.61	-254.8	2305
5.00	-23.50	-316.4	2995
5.55	-	-377.5	3750
6.10	-28.43	-510.3	5675

[a]Standard deviation = 0.15

[b]Standard deviation ≤ 1.7

[c]Standard deviation ≤ 20

List of Figures

4. (c) A normalized sulfur XANES spectrum of the bulk peat sample. Least squares fitting was optimized from 2465 to 2490 eV. Model S XANES spectra and their percent contribution to the fit are shown in Fig. A.5.

Figure 9. Principle component analysis of the sulfur μX-ray fluorescence (μXRF) maps collected at energies of 2470, 2472, 2473.5, 2474.5, 2482.5, and 2500 eV on the peat grain displayed in Figure 8a. Components 1 through 6 are displayed in (a) through (f), respectively.

Figure 10. (a) Sulfur μXRF mapped at 2500 eV of the peat grain in Figure 8a. Warmer colors indicate higher sulfur fluorescence intensity. Numbers indicate the locations where sulfur μXANES spectra were collected. (b) Normalized sulfur μXANES spectra with least squares fitting results optimized from 2465 to 2490 eV using model spectra (Table A.1). Model organic sulfur species include cystine, diphenylsulfide, diphenyldisulfide, dibenzyldisulfide, diphenylsulfoxide, dimethylsulfoxide, and a sulfate ester (Fig. A.4).

Figures

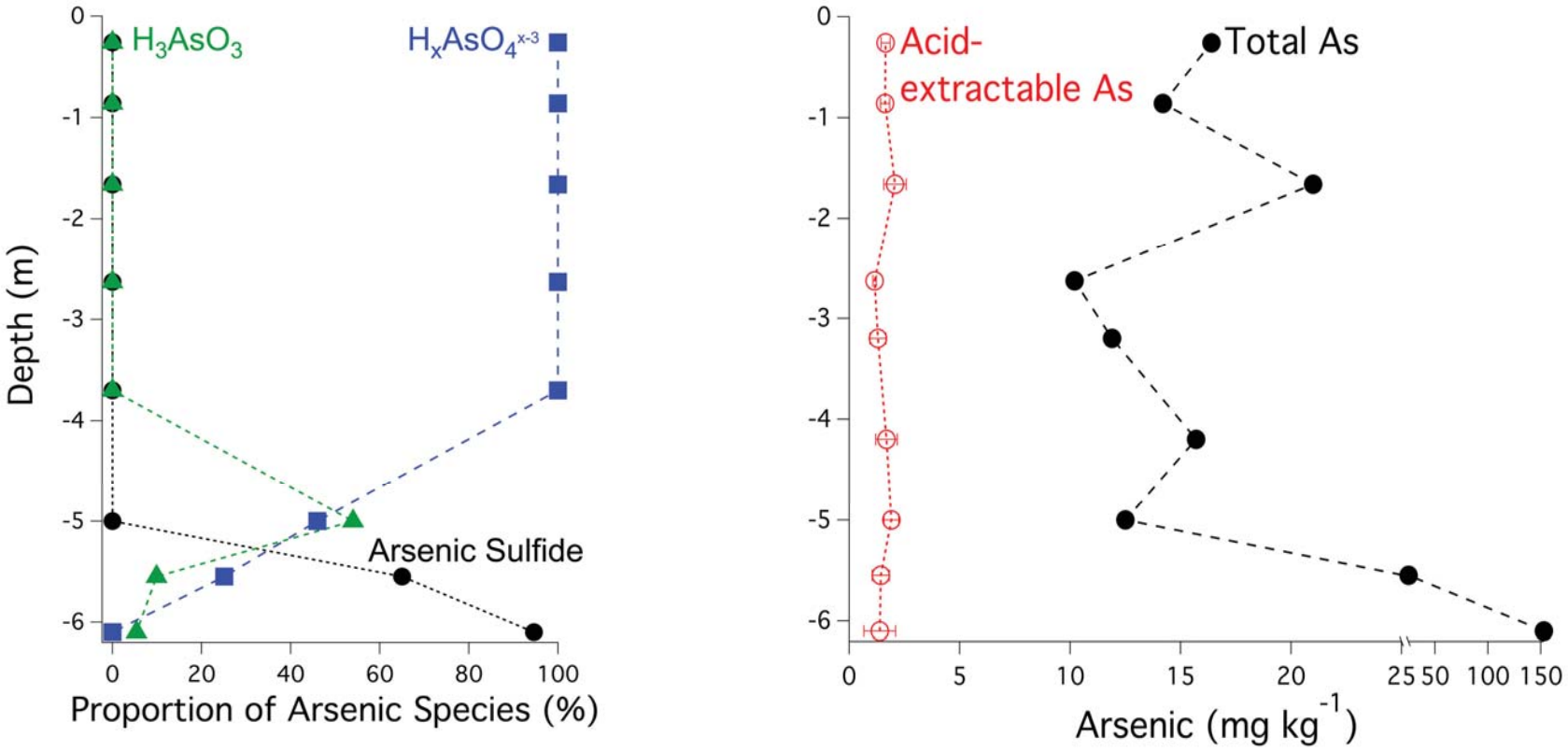

Figure 1

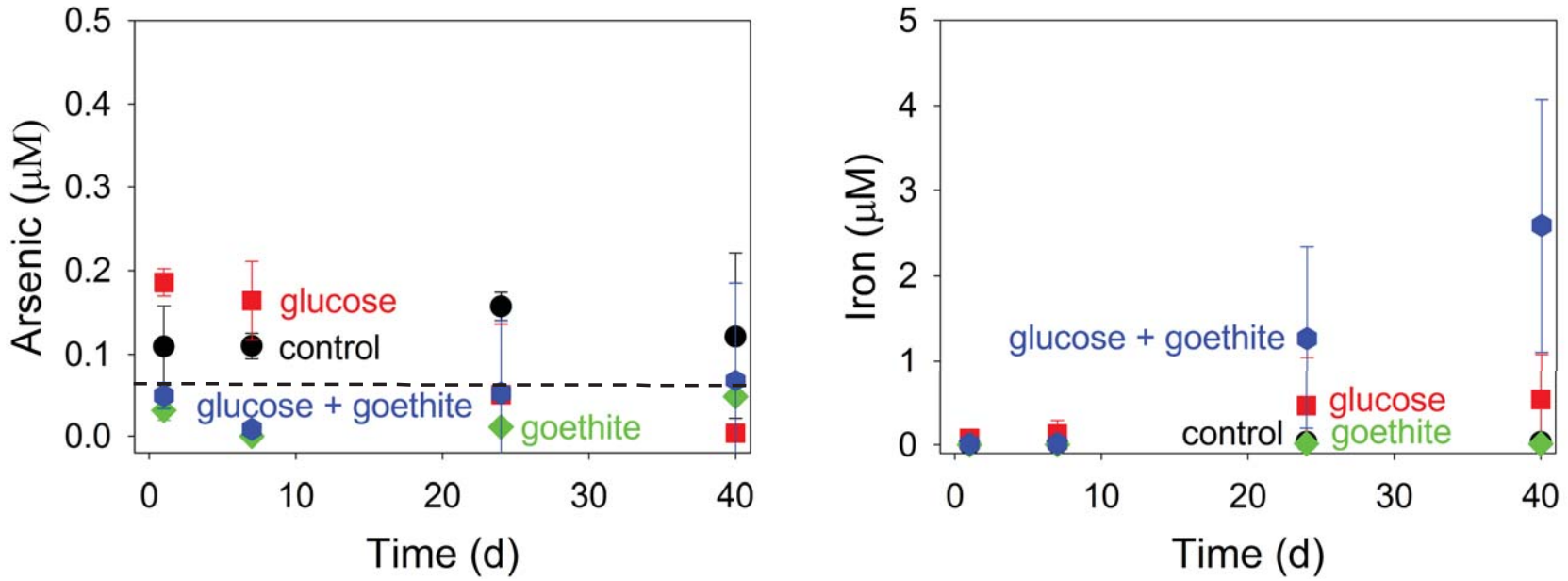

Figure 2

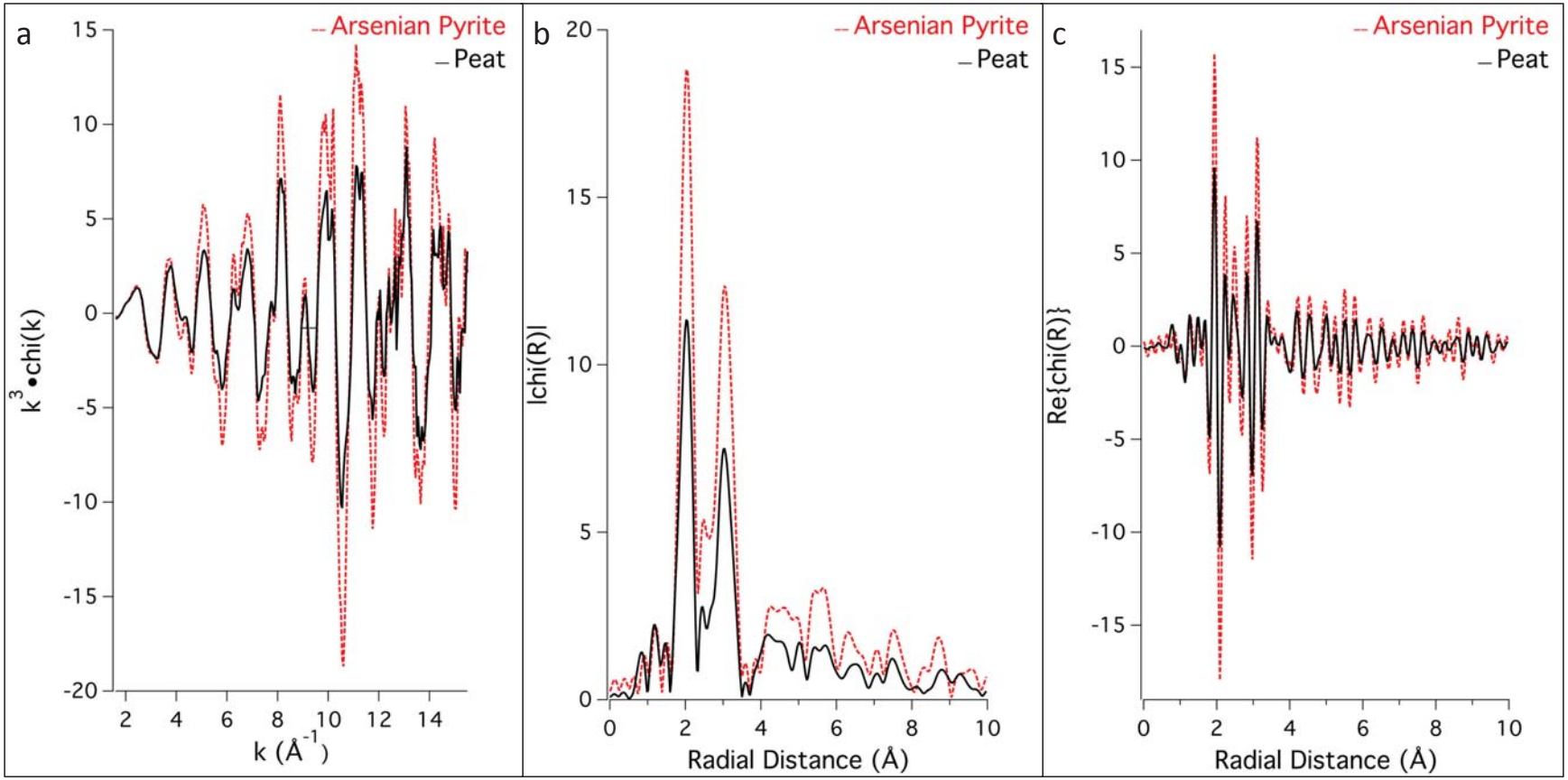

Figure 3

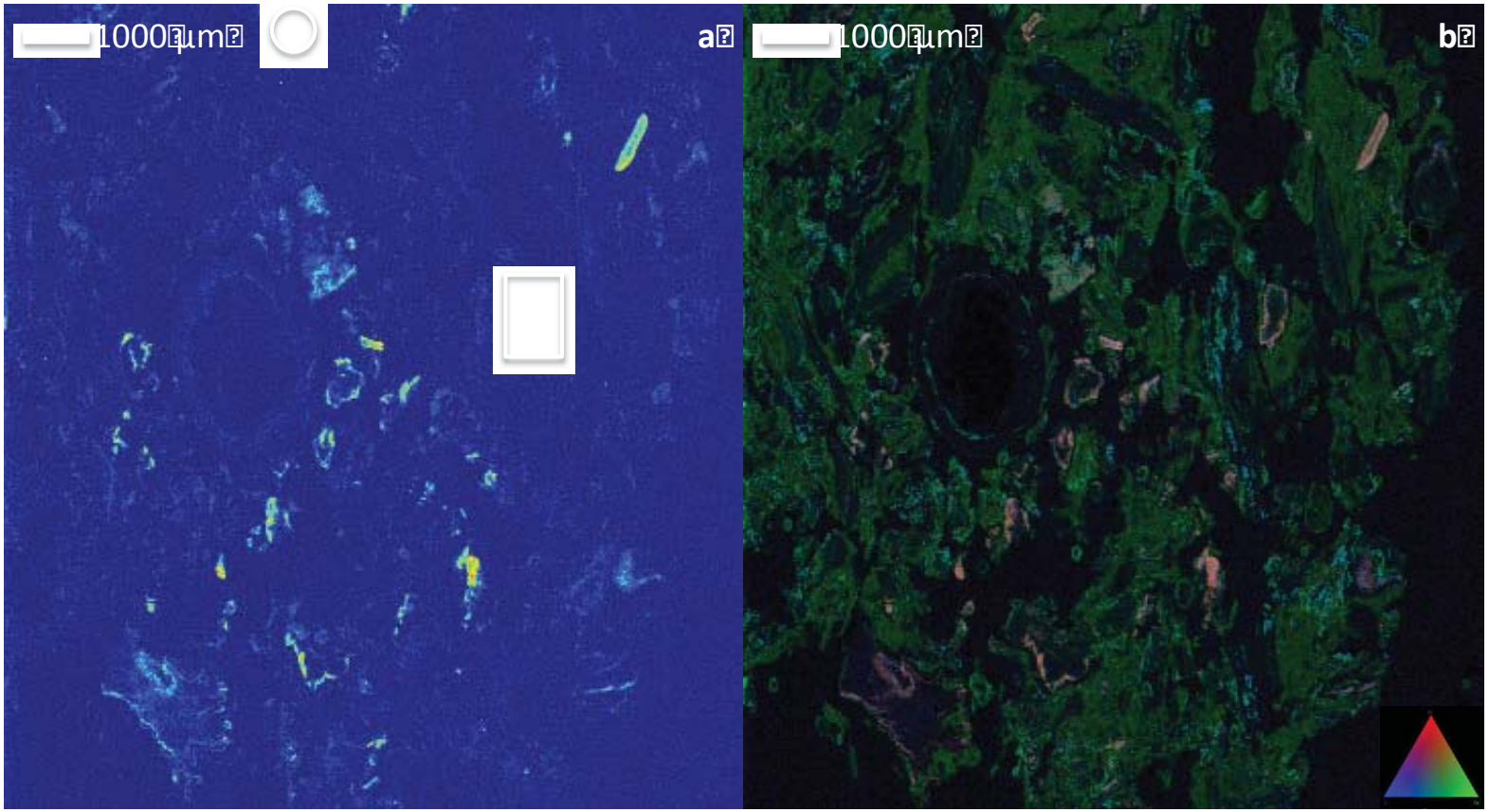

Figure 4

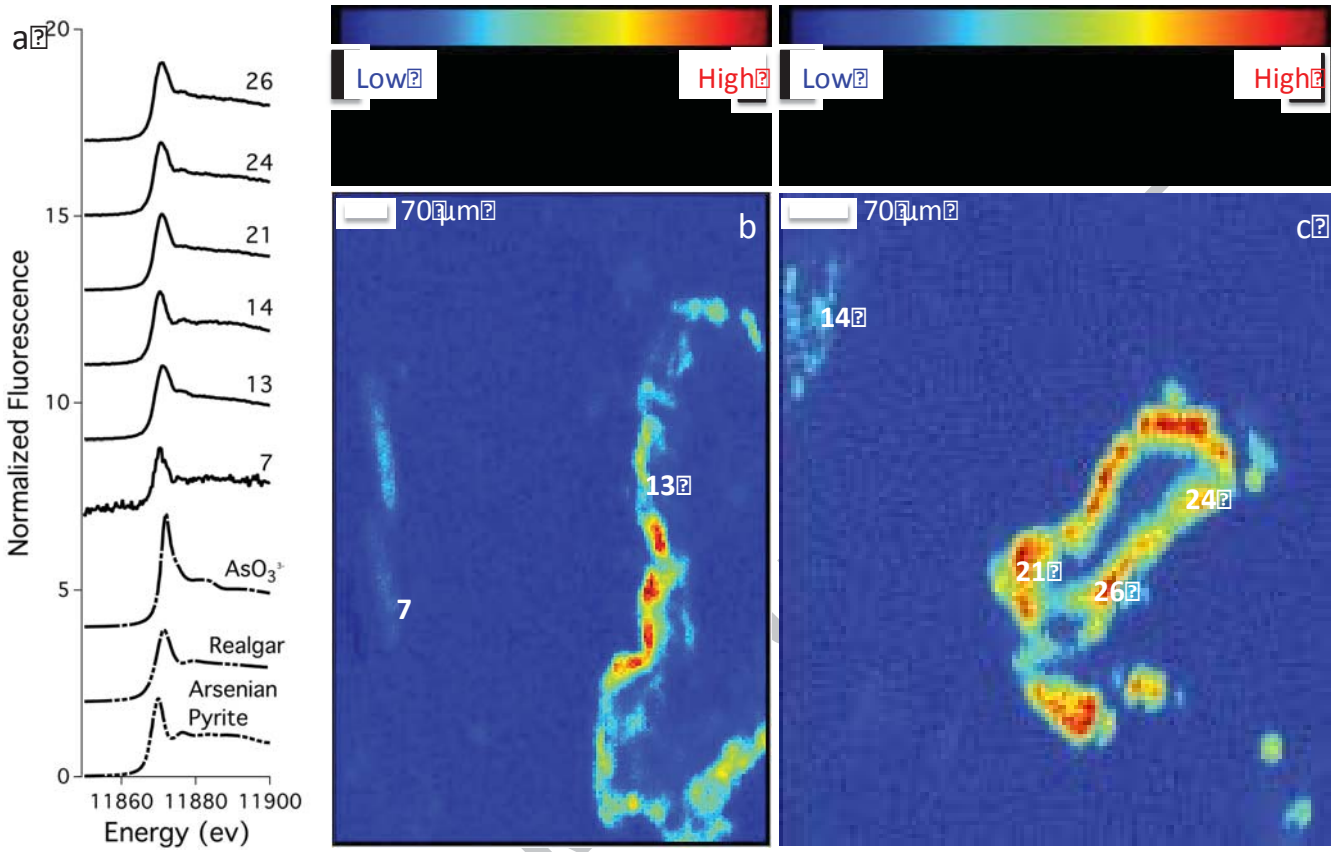

Figure 5

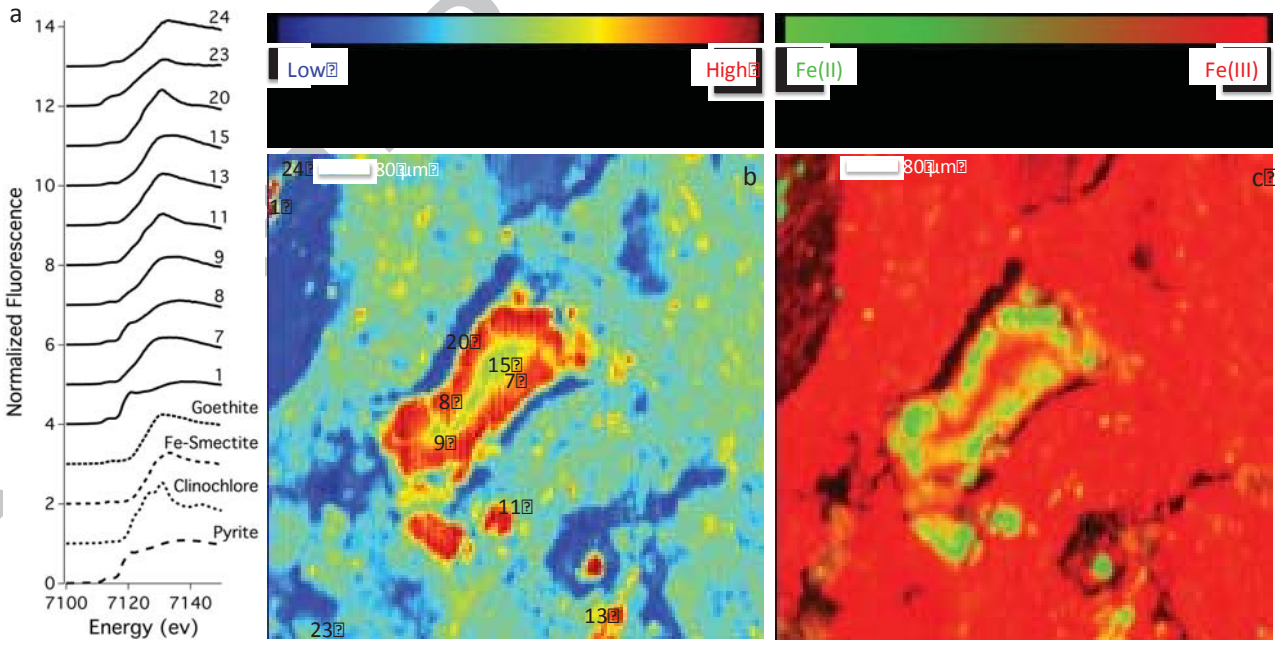

Figure 6

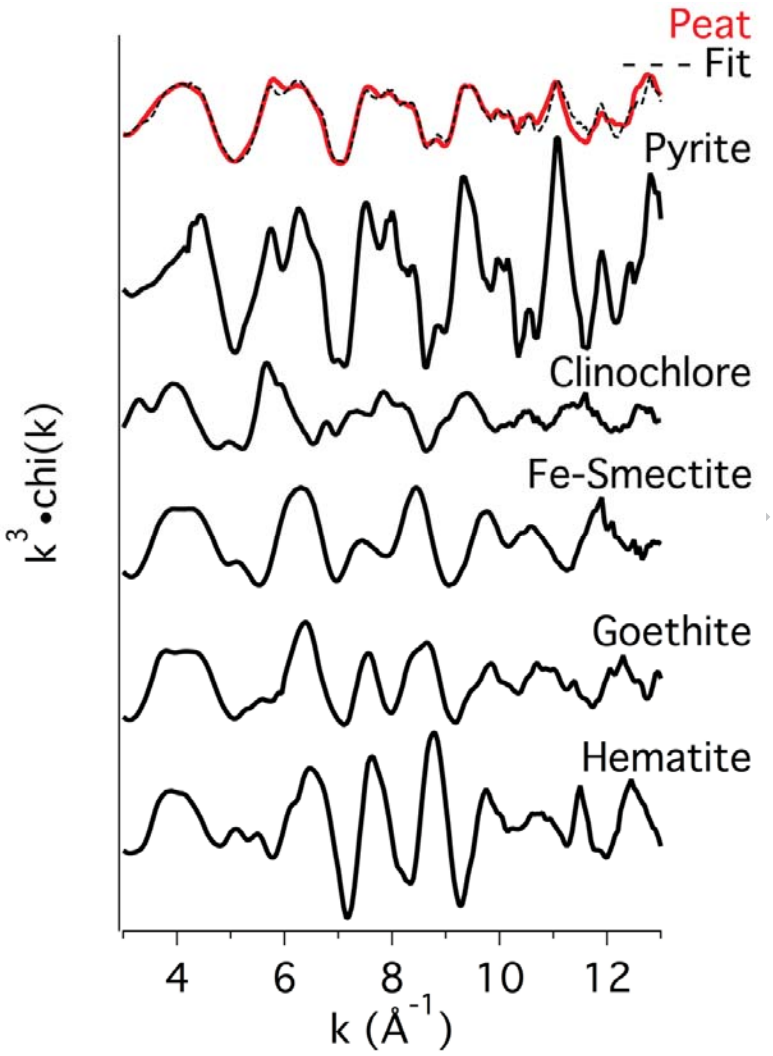

Figure 7

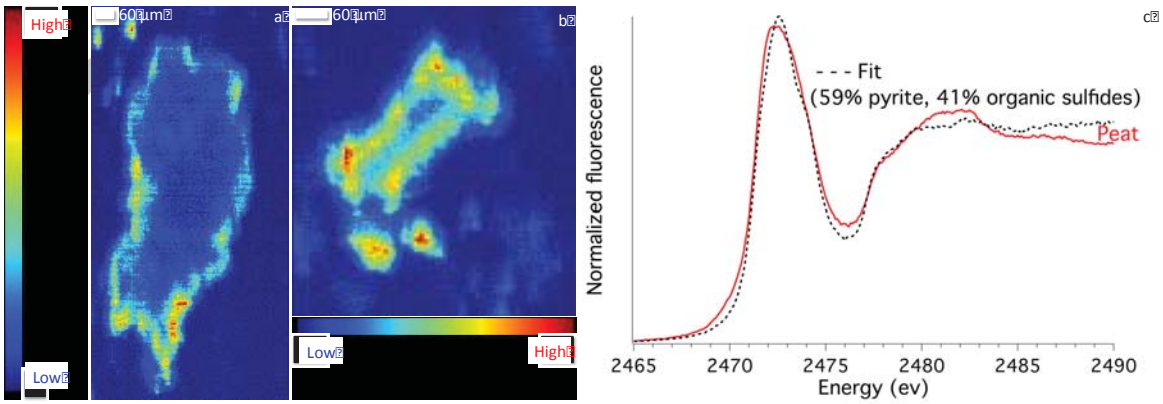

Figure 8

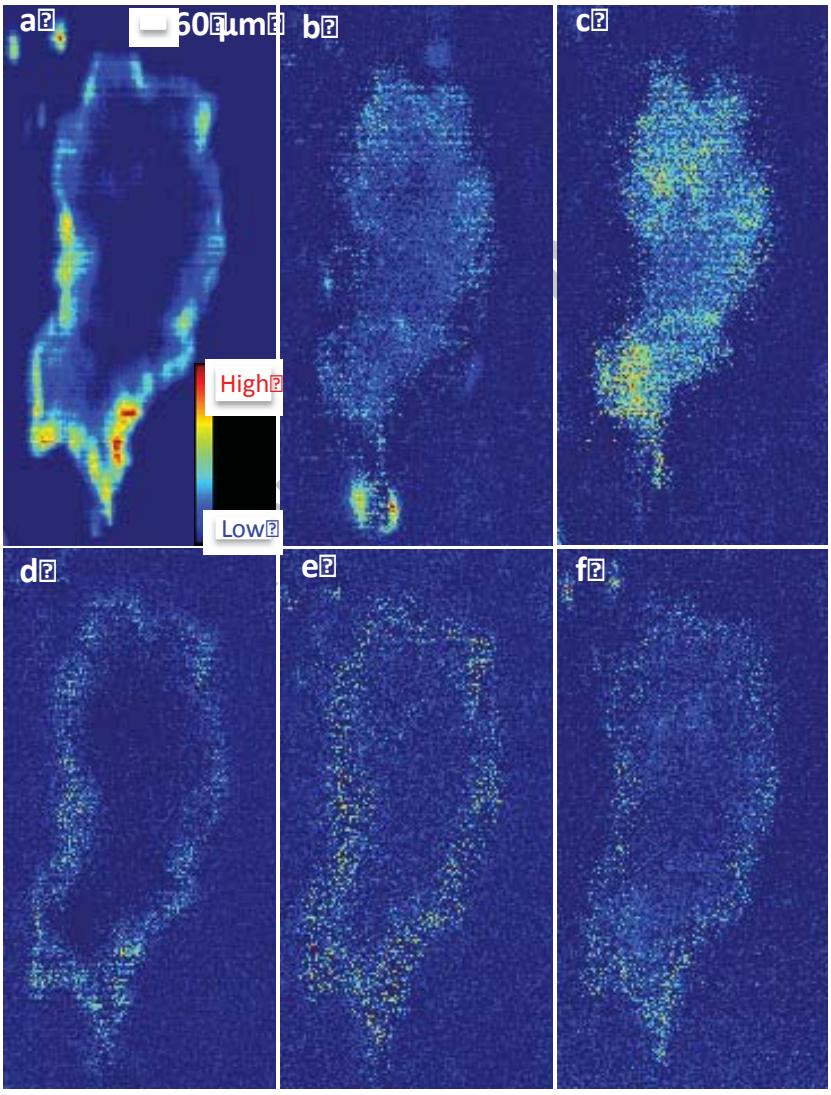

Figure 9

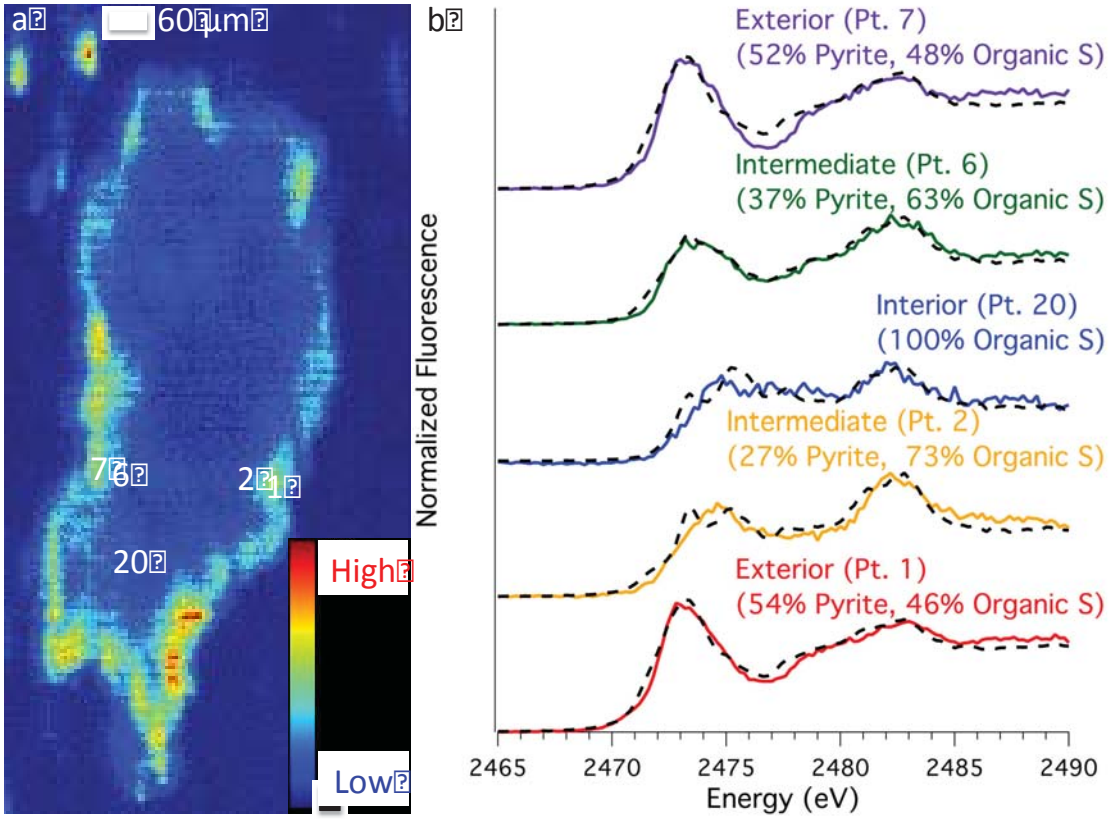

Figure 10